Recombination Suppression in PbS Quantum Dot Heterojunction Solar Cells by Energy-Level Alignment in the Quantum Dot Active Layers

著者	Ding Chao, Zhang Yaohong, Liu Feng, Nakazawa Naoki, Huang Qingxun, Hayase Shuzi, Ogomi Yuhei, Toyoda Taro, Wang Ruixiang, Shen Qing
journal or publication title	ACS Applied Materials & Interfaces
volume	10
number	31
page range	26142-26152
year	2017-09-01
URL	http://hdl.handle.net/10228/00006895

doi: info:doi/10.1021/acsami.7b06552

Recombination Suppression in PbS Quantum Dot Heterojunction Solar Cells by Energy Level Alignment in the Quantum Dot Active Layers

Chao Ding,[a,e] Yaohong Zhang,[a] Feng Liu,[a] Naoki Nakazawa,[a] Qingxun Huang,[a] Shuzi Hayase, [b,] [d] Yuhei Ogomi,[b] Taro Toyoda,[a,d] Ruixiang Wang,[c] Qing Shen[a,d]*

a. Faculty of Informatics and Engineering, The University of Electro Communications, 1-5-1 Chofugaoka, Chofu, Tokyo 182-8585, Japan.

b. Faculty of Life Science and Systems Engineering, Kyushu Institute of Technology, 2-4 Hibikino, Wakamatsu-ku, Kitakyushu, Fukuoka 808-0196, Japan.

c. Beijing Engineering Research Centre of Sustainable Energy and Buildings, Beijing University of Civil Engineering and Architecture, No.15 Yongyuan Road, Huangcun, Daxing, Beijing 102616, China.

d. CREST, Japan Science and Technology Agency (JST), 4-1-8 Honcho, Kawaguchi, Saitama 332-0012, Japan.

e. China Scholarship Council Address: Level 13, Building A3 No.9 Chegongzhuang Avenue Beijing 100044, China.

KEYWORDS: lead sulfide (PbS), quantum dot heterojunction solar cells (QDHSCs), energy level alignment (ELA), recombination mechanism, recombination suppression.

ABSTRACT: Using spatial energy level gradient engineering with quantum dots (QDs) of different sizes to increase the generated carrier collection at the junction of a QD heterojunction solar cell (QDHSC) is a promising strategy for increasing the energy conversion efficiency. However, the results of current related research have shown that a variable band gap structure in a QDHSC will create an appreciable increase not in the illumination current density but rather in the fill factor. In addition, there is a lack of studies on the mechanism of the effect of these graded structures on the photovoltaic performance of QDHSCs. This study presents the development of air atmosphere solution-processed TiO_2/PbS QDs/Au QDHSCs by engineering the energy level alignment (ELA) of the active layer via the use of a sorted order of differently sized QD layers (4 QD sizes). Compared to the ungraded device (without the ELA), the optimized graded architecture (containing the ELA) solar cells exhibited a great increase (21.4%) in short-circuit current density (Jsc). As a result, a Jsc value greater than 30 mA/cm^2 has been realized in absorption layer thinner （~300nm） planar PbS QDHSCs, and the open-circuit voltage (Voc) and power conversion efficiency (PCE) were also improved. Through characterization by the light intensity dependence of the Jsc and Voc and transient photovoltage decay, we find that: (i) The ELA structure, as an electron-blocking layer, reduces the interfacial recombination at the PbS/anode interface; (ii) The ELA structure can drive more carriers towards the desirable collection electrode, and the additional carriers can fill the trap states, reducing the trap-assisted recombination in the PbS QDHSCs. This work has clearly clarified the mechanism of the recombination suppression in the graded QDHSCs and demonstrated the effects of ELA structure on the improvement of Jsc. The charge recombination mechanisms characterized in this work would be able to shed light on further improvements of QDHSCs and/or other types of solar cells.

1.INTRODUCTION

Quantum dot solar cells (QDSCs), as a very promising candidate for next-generation solar cells, have attracted much attention. This is mainly because of the many advantages of QDs, such as their bandgap tunability due to the quantum size effect, facile solution processing, and multiple exciton generation (MEG) as well as their effect of slowing down the cooling of hot electrons.[1-3] Due to the large (18 nm) Bohr radius of lead sulfide (PbS), PbS QDs have a broadly tunable bandgap in the size range of 3–5 nm, making them competitive for photovoltaic applications.[4] Since the first near-infrared-absorbing (λ > 800 nm) colloidal QDSCs were reported,[5] PbS quantum dot heterojunction solar cells (QDHSCs) have developed rapidly as a result of the efforts focused on advanced QD surface engineering and designing and improving device architectures.[6-8] In QDHSCs, normally, ZnO or TiO_2 thin films deposited on transparent electrodes (such as FTO) are used as electron transport layers, PbS or PbSe QDs are employed as the optical absorption layer, and Au deposited on the surface of the QD layers is used as an electrode to collect holes. To date, PbS QDHSCs with efficiencies of more than 10%[9-10] have been based on engineering the band alignment of two QD layers as well as better passivation using molecular halides.[6] The success originally depended on the reasonable tuning of energy level alignments (ELAs) between different PbS QD layers treated with different ligands. Tuning the ELA serves as the main route to improve the efficiencies of QDHSCs, mainly through two approaches: size-tunable bandgaps[11-16] and ligand chemistry.[6] In addition, using graded doping[17] and surface dipole moments[18] to tune the ELA to improve the performance in QDHSCs was demonstrated.

ELA within the light-absorbing, charge-transport active layer has previously been used in epitaxial compound semiconductor thin films such as GaAs and $CuIn_xGa_{1-x}Se_2$ thin film solar cells.[19-21] In those studies, ELA could improve photovoltaic (PV) performance through a number

of mechanisms and in a variety of materials. For example, it could facilitate carrier collection, strengthen the built-in electric field, and improve the fill factor (FF), short-circuit current (Jsc) and open-circuit voltage (Voc). As a result, improved photovoltaic conversion efficiencies have been experimentally demonstrated. However, the procedure to process the ELA structure in a thin film solar cell is complicated, and it is difficult to fabricate an efficient barrier layer between the window layer and the back-electrode layer to reduce electron and hole carrier recombination. Above all, in the thin film layer, the composition variation can easily generate many bulk traps due to the lattice mismatch.[22] As a result, the range of bandgap grading is greatly limited. In addition, current matching is required to optimize the thin film solar cells, which requires theoretical calculations and a large number of experimental practices.[21]

Compared with the preparative techniques of the abovementioned compound semiconductor thin film solar cells, the use of size-tunable QDs to prepare ELA solar cells is a good alternative. Tuning the ELA by simply adjusting QD sizes is an advantage of QD-based solar cells and is very easily achievable. Stacking multiple layers of QDs with different sizes need not to consider the lattice matching at the interfaces of QD layers, because the QDs are passivated by ligands and do not directly contact with each other. The bandgap-ordered QD layers can be created via a layer-by-layer spin coating process, and this method can be used to easily control the spatial bandgap variation according to a design. In the QDHSCs, ELA has been used to improve carrier transport and collection, which can be ascribed to the quantum funnel effect, i.e., the ELA structure drives the performance-limiting electrons towards the electron-accepting electrode, resulting in the efficient collection of photogenerated carriers.[13] However, previous research results [11, 13, 16] showed that the ELA structure solely leaded to an increase in FF rather than an appreciable increase in Jsc

as expected. In addition, after inserting the ELA structure in standard QDHSCs, changes in the transport as well as the recombination mechanism of carriers are not clear.

In our work, we have designed an ELA architecture (i.e., the graded structure) through interface engineering by using different QD size layers in order to explore the effect of ELA on the photovoltaic performance of PbS QDHSCs. We found that the ELA structure can enhance Jsc greatly. Compared to an ungraded device (without the ELA), the optimized graded architecture (containing the ELA) solar cells exhibited a great increase (21.4%) in Jsc. A Jsc value greater than 30 mA/cm^2 has been realized in the PbS QDHSCs, and a high efficiency of 7.25% has been achieved. We have investigated the mechanism through characterization of Voc decay and light intensity dependences of Voc and Jsc. We have clearly demonstrated that enhancement of Jsc in the QDHSCs result from reducing the recombination at both the QD active layer and the interface using the ELA structure. Furthermore, the performance of unencapsulated PbS QDHSCs remained stable for over 150 days of storage in air. The most important thing is that all of the PbS quantum dots at each layer are passivated with inorganic ligands in our devices without using 1,2-ethanedithiol (EDT) which is normally used, and all of the processes including preparation, characterization and store of the devices are carried out under air condition.

2. RESULTS AND DISCUSSION

In this work, different sizes of PbS QDs were synthesized using a modified hot-injection method,[23] and four sizes of PbS QDs were prepared by controlling the injection temperature. Figure 1a shows the absorbance spectra of PbS QDs with the different sizes. The spectra demonstrate that the synthesis allows the preparation of QDs with a first excitonic absorption peak varying between 1055 and 750 nm (the first excitonic energy or bandgap Eg: 1.17–1.63 eV). The diameter (d) of the PbS QDs is calculated using equation (1).[24] This equation allows us to

determine d directly from Eg, avoiding a lengthy transmission electron microscopy (TEM) analysis for each sample synthesized. The calculated sizes of the QDs are 2.6–3.6 nm, and the four sizes of PbS were denoted M (3.6 nm), S1 (3.3 nm), S2 (2.9 nm), and S3 (2.6 nm).

$$E_g = 0.41 + \frac{1}{0.252d^2 + 0.283d} \qquad (1)$$

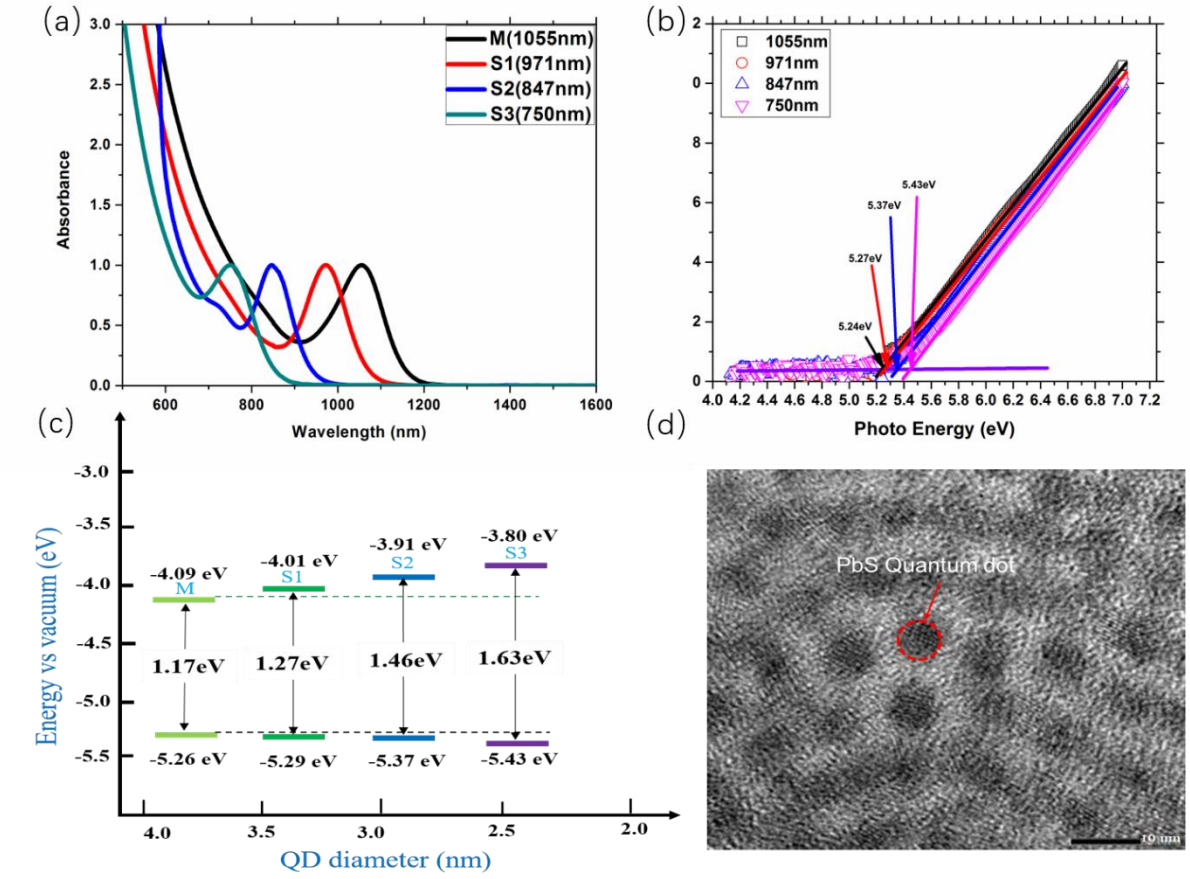

Figure 1. (a) The absorption spectra of the PbS QDs in octane. (b) Photoelectron yield (PY) spectra of the PbS QDs. (c) The energy level diagram of the PbS QDs of different sizes. (d) A TEM image for PbS QDs with the first excitonic energy Eg of 1.17 eV.

In this work, the valence band maximum (VBM) of the four sizes of PbS QDs were measured by using photoelectron yield (PY) spectroscopy, as shown in Figure 1b. As the PY signal intensity

has a good S/N ratio, the error bars are included within the points. The VBM edge is determined from the intersection of the baseline with the tangent to the spectra. Then, by combining the results of both of band gap Eg and VBM, the energy levels of the conduction band minimum (CBM) were determined, as seen in Figure 1c. We can observe that the energy levels of both CBM and VBM obviously change with the PbS QD sizes, which is in agreement with those results reported by Miller et al.[25] Miller and co-workers reported that the standard way for analyzing the VBM using XPS/UPS may be not correct for larger size QDs due to the extremely low density of states at the VBM. But in our work, smaller size PbS QDs are used and thus the PYS results could be expected to be reliable. Based our measured PYS results, we can assume that in the 2.6–3.6 nm range, the changes in the VBM are smaller than those in the CBM as the size of the QDs varies. Thus, changes of size within a certain range can tune the conduction band energy at the top of the absorber layer for the constructed ELA structure of the PbS QDHSCs. In addition, for the PbS QDHSCs, it was confirmed that the 3–5 nm range translates into the broad optimal efficiency bandgap peak.[26] Thus, we can use these four sizes of PbS QDs to build an ELA structure. Figure 1d shows a typical TEM image of M-size PbS QDs, illustrating that the PbS QDs are spherical and that their diameter is very close to the calculated one.

In this work, we design and characterize an ungraded device and three types of graded devices with different electron collection efficiencies. Figure 2 illustrates spatial band diagrams of the photoelectron cascades within the solar cells studied here. In our previous report,[27] solar cells employing PbS QDs with a first excitonic absorption peak at a wavelength λ = 1050 nm (first exciton energy Eg of 1.17 eV) showed high performance, and thus the PbS QDs with this absorption peak were employed to fabricate the ungraded device and the base layer of the graded devices, and other smaller-diameter QDs (Figure 1a) were employed to build the upper layers. The

active layer of Type I (ungraded device) had a thickness of approximately 300 nm, an optimized thickness that achieved the best efficiency (as shown in Figure S1) and the bulky ligands of the PbS QDs were replaced with short ligands through a hexadecyltrimethylammonium bromide (CTAB) treatment.[27-28] All processes were performed under ambient conditions. For the devices using ELA engineering, the active layers of the three types of graded devices contained two, three and four compositions, respectively. Type II consisted of a 260-nm-thick film of M-PbS QDs (1.17 eV) deposited on the TiO_2 compact layer with a subsequent 40-nm-thick layer of S2-PbS QDs (1.46 eV); Type III consisted of a 220-nm-thick layer of M-PbS QDs with subsequent successive 40-nm-thick layers of S1-PbS (1.27 eV) and S2-PbS QDs; and Type IV consisted of a 180-nm-thick layer of M-PbS QDs with subsequent successive 40-nm-thick layers of S1, S2 and S3-PbS QDs (1.63 eV). Therefore, the thickness of the total active QD layers is ~300 nm for all the device types.

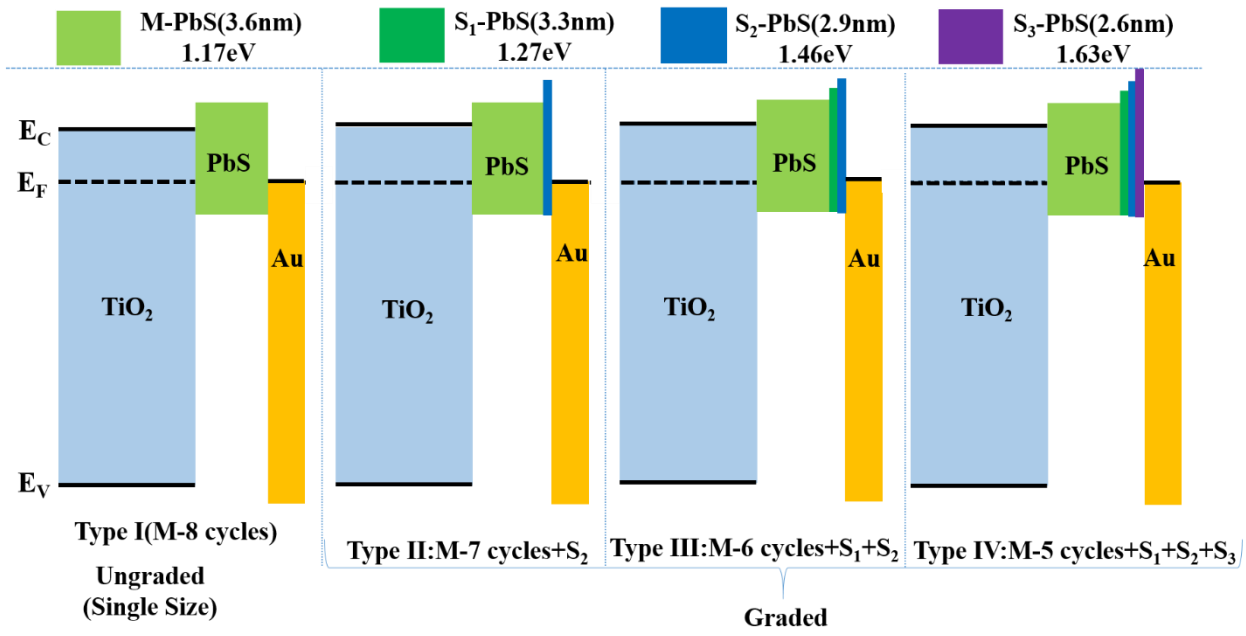

Figure 2. Spatial band diagrams of ungraded and 3 types of graded QD solar cells. Color coding corresponds to larger bandgaps (more blue/violet). Type I: a thickness of ~300 nm the active layer

with M-PbS QDs, Type II:M-PbS (~260 nm) +S2-PbS (~40 nm), Type III:M-PbS (~220 nm) +S1-PbS (~40 nm) +S2-PbS (~40 nm). Type IV: M-PbS (~180 nm) +S1-PbS (~40 nm) +S2-PbS (~40 nm) +S3-PbS (~ 40 nm).

As an example, Figures 3a and b show the schematic structure and a cross-sectional scanning electron microscopy (SEM) image, respectively, of a Type III graded solar cell with an Au electrode on the PbS QD layer. The low-temperature-processed TiO_2 compact layer acts as an electron-accepting/hole-blocking layer. The bottom six cycles of the CTAB-passivated QD layer of this structure utilize the M-PbS QDs as the main charge generation layer, followed by single layers of CTAB-passivated S1 and then S2-PbS QDs as a spatial gradient ELA structure (Figure 3a). The cross-sectional SEM image of a typical Type III device (Figure 3b) shows an ~35-nm-thick TiO_2 layer and an ~ 300-nm-thick QD layer. In addition, the layer-by-layer process keeps each CQD layer fused together, rather than producing distinctly stratified interfaces.

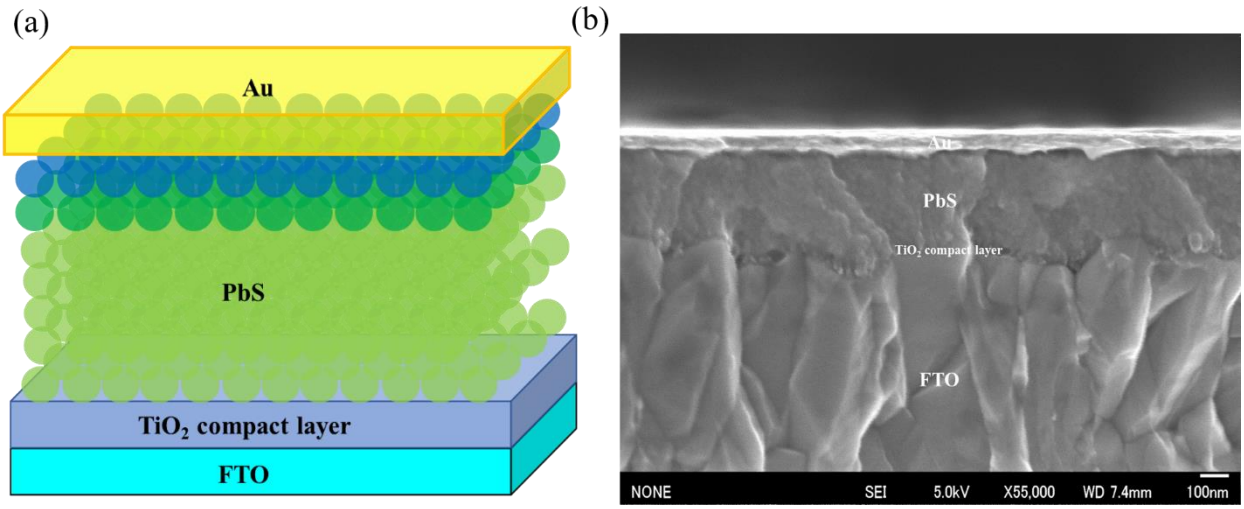

Figure 3. (a) Schematic illustration of graded device Type III structure. (b) Cross-sectional SEM image of a typical device of type III (~300 nm thick PbS QD active layer).

Figure 4a show the typical photocurrent density–voltage (J–V) characteristics of the four types of QDHSCs under 1 sun-illumination. We have measured 24 devices for each type of the QDHSCs. The average values of the photovoltaic parameters such as Voc, Jsc, FF, series resistance (Rs), shunt resistance (Rsh), and PCE are shown in Table 1. In addition, the champion results of each type of the QSHSCs are shown in the parentheses of Table 1. Compared with the ungraded device (Type I), the graded devices (Types II, III) show desirably increased power conversion efficiencies (PCEs) that originate from the significant improvements in Jsc (~ 20% increase). From the J–V results, by employing different numbers of graded structure layers, we found that Types II and III of the ELA structure yielded an optimum result in this system and that an additional differently sized layer yielded no further benefits in photovoltaic properties. Remarkably, under 1-sun illumination, the best performance by a graded Type III QD device showed a Jsc of 32.65±1.03 mA/cm^2, Voc of 441±8 mV, FF of 46±2% and PCE of 7.12 ± 0.11%.

Table 1. Statistical average of the photovoltaic performance parameters of 24 devices for each type of the QDHSCs. The champion results are shown in the parentheses.

Sample	Voc (mV)	Jsc (mA·cm^{-2})	FF (%)	PCE (%)	Rs (Ω·cm^2)	Rsh (Ω·cm^2)
Type I	427 ±9 （438）	25.82±1.39 （27.81）	48±1 （50）	6.12±0.13 （6.28）	4.56±1.14 （4.73）	111.4±11.7 （121.4）
Type II	438 ±8 （448）	30.92±1.12 （32.54）	46±2 （49）	6.82±0.12 （7.02）	5.88±1.76 （6.1）	124.2±17.6 （135.4）
Type III	441 ±8 （451）	32.65±1.03 （33.58）	46±2 （48）	7.12±0.11 （7.24）	7.28±2.16 （7.94）	677.9±19.2 （691.3）
Type IV	450 ±9 （462）	28.88±1.17 （30.29）	42±1 （44）	6.10±0.09 （6.22）	10.28±1.89 （10.57）	726.8±14.8 （736.1）

The trend of improving performance with the ELA structure depended on two aspects: Jsc and Voc. The most important improvement was that the average (as shown in Figure S2, 24 samples) Jsc was enhanced in the graded device compared to the ungraded one. The Jsc improved to 32.65 ±1.03（33.58）mA/cm^2 (Type III) compared to 25.82±1.39 mA/cm^2 (Type I), and the Voc also slightly increased from 427 ±9 mV (Type I) to 450 ±9 mV (Type III) with the added layer of the ELA structure, while the FF decreased to 46±2 % (Type III) from 48±1% (Type I). However, for the added three layers of differently size QDs (Type IV), we observed decreased efficiency due to the deteriorated Jsc and FF compared to the Type III solar cell.

The dark J-V characteristics of the four types of QDHSCs are shown in Figure 4b, which suggest that the increasing number of ELA structure layers leads to an increase in series resistance (Table 1). Resistive losses are believed to be the main reason for the reduced FFs observed in the QDSCs.[29] The increased series resistance may arise from the valence band offset between the absorber layer (M) and the top layer (Sn, n=1, 2, 3), which causes a weak effect that blocks hole diffusion to the metal contact (Au), and a hole accumulation layer, which forms a weak barrier at the upper layer of the ELA structure. This barrier reduced hole collection in the graded devices compared with the ungraded device and caused interfacial effects at the metal contacts (Figure S3). Therefore, we used three differently sized PbS QDs to prepare three kinds of Type II model graded structure devices and measured their dark current characteristics. The results indicate that the series resistance increased with increasing valence band offset (Figure S4), revealing a reduction in hole transport to gold electrode due to increasing hole-blocking effect.

Our experimental results and the previously reported results clearly differ.[11, 13, 15-16] In our graded devices, Jsc can be increased to very high values, but FF deteriorates. The external quantum efficiency (EQE) spectra of the four types of QDHSCs are shown in Figure 4c. The EQE values

of the graded devices are much larger than those of the ungraded device. On the other hand, the optical absorption spectra (Figure S5) show that the optical absorption of the graded devices are not larger than that of the ungraded device. Therefore, the improvements of the EQE and Jsc of the graded devices are not attributable to an enhancement of the light absorption, which has also been confirmed by other groups.[14] We believe that the greater EQE of the graded devices is due to the quantum funnel effect [13] resulting from the ELA structure.

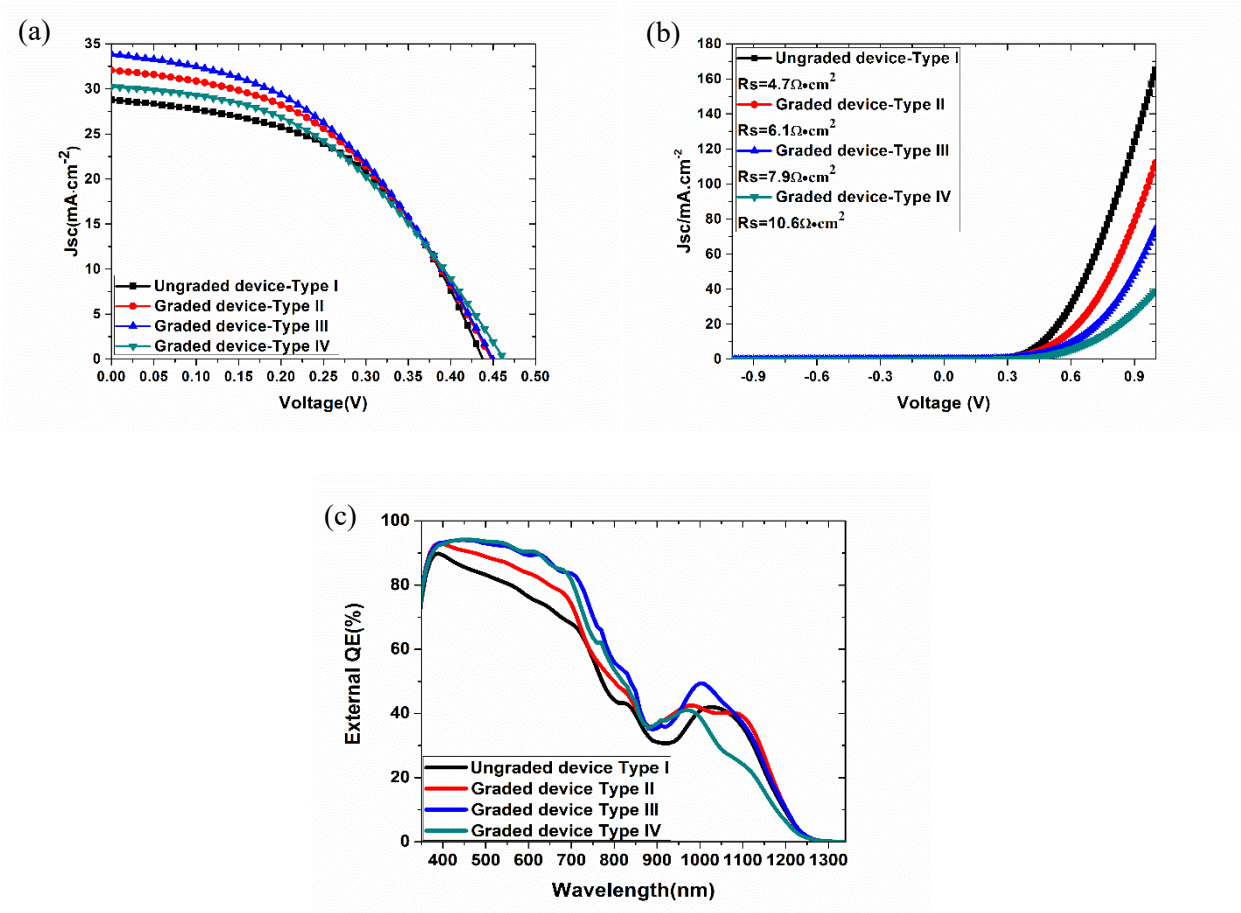

Figure 4. (a) J-V characteristics under simulated AM 1.5G illumination for the ungraded and three types of graded devices. (b) The dark current characteristics of these devices. The series resistances (RS) were extracted by fitting these dark current characteristics by a single diode model.[29] (c) External quantum efficiency (EQE) spectra for the ungraded and three types of graded devices.

From the spatial band diagrams (Figure 2), the upper layer of both the Type II and Type III devices is the same, i.e., an S2-PbS QDs layer. Although the Jsc values of the two types of devices both increased, Type III has a higher Jsc. This result shows that for the Type II device, the role of the ELA structure is mostly to effectively block electrons, but the ELA structure of the Type III device, in addition to blocking electrons, also provides a multi-stage impetus to drive minority carriers generated at these depths towards the desired electrode. In order to further confirm this, we have compared the photovoltaic performances of the ungraded device (Type I), the graded device (Type III) and a new device which only contains an electron blocking layer (EBL) of PEDOT: PSS. The QD active layers are same for these three devices as shown in Fig. S6. Here, we chose PEDOT: PSS as electron blocking layer material is because that PEDOT: PSS has the very good band energy level matching as an EBL (as shown in Figure S6a) for the PbS QDs used in the active layer. As shown in Figure S6b, c and Table S1, it is very clear that the photovoltaic performance has been enhanced significantly by the ELA structure (graded Type III device) compared to the device employing the EBL layer only. This result demonstrates that the graded energy level structure does contribute to the improvement of the solar cell performance, but the improvement is not merely due to the formation of electron blocking layer.

Through integrating the EQE spectra with the AM1.5G solar spectrum for the four champion QDHSC types, values of Jsc were calculated as 26.7 ± 0.92 and 30.7 ± 1.07mA/cm^2, respectively, in good agreement with the measured J–V results (25.82 ± 1.39 and 32.65 ± 1.03 mA/cm^2). These results also suggest that the Jsc of these planar PbS QDHSCs with a PbS layer thickness of only approximately 300 nm can more closely approach the Jsc of depleted-bulk-heterojunction-structured PbS QDSCs, in which the active layer thickness is normally larger than 1000 nm (e.g., ZnO nanowires/PbS)[27, 30] The Jsc more than 30 mA/cm^2 in planar PbS QDHSCs were also reported

by other two strategies[28, 31]. One strategy is that a cascaded-junction quantum dot solar cell was fabricated by using 3 kinds of sizes of highly monodispersed PbS QDs. [31] In the device, one layer of larger size PbS QDs with TBAI ligand was placed between ZnO and QD active layer to reduce the interfacial recombination at ZnO/QD interface and to decrease leakage current. [31] Then, one layer of smaller size PbS QDs with EDT ligand was placed between the QD active layer and the Au electrode as an electron-blocking/hole-extraction layer to decrease recombination at this interface. However, the organic ligand EDT passivated PbS quantum dot layer would have a negative influence on the illumination stability of device under air condition[32,33]. Almost all of the PbS QDHSCs using EDT as passivation ligands were measured in N_2 atmosphere rather than in air[6, 9, 34-35]. In another strategy, a new-ligand (pseudohalogens) was employed for PbS QD surface passivation and a thick QD active layer (more than 500 nm) was used, which increased the Jsc largely[28]. In our devices, although the thickness of the active layer is only about 300 nm, Jsc values greater than 30 mA/cm^2 have been realized, which is originated from the ELA structure. The most important thing is that all of the PbS quantum dots at each layer are passivated with inorganic ligands (Br-) in our devices, and all of processes including preparation, characterization and store are carried out under air condition in this work.

For our graded devices, the conduction band energy gradient produces an additional driving force for electrons, and the degree of band bending (the conduction bandgap variation with position) is in the order of Type IV > Type III > Type II. Figure 4c shows that the EQE of the graded devices increased as the quantum funnel effect strengthened in the visible and long-wavelength range (400–1050 nm). This is because of the decreased recombination rate caused by the enhanced separation of the electrons and holes due to the driving force originating from the internal electric field and the ELA. In other words, the ELA structure causes an increased gradient in the carrier

profile (i.e., an effective larger intrinsic electric field), and thus, the recombination rate decreases; this explains the further enhancement in EQE for the graded devices. In this work, the EQE spectrum shows that the improvement in Jsc in the graded device is mainly due to the visible light range of the photoelectric conversion, although the optical absorbance in the visible region is almost the same for the four devices. This result indicates that the charge collection efficiency decreases in the order of Type IV > Type III > Type II > Type I. The decrease in Type IV EQE in the 1000–1200 nm spectral range may be partly attributed to the decrease in the optical absorbance due to the thinner active layer thickness as shown in Figure S5.

As shown in the above results, the Jsc and Voc both increased by introducing the ELA structures, which indicates that the extracted current is increased and recombination within the quasineutral region is reduced, so the optimized ELA structure can increase the diffusion length such that it is longer than the quasineutral region. To explore the mechanism of the photovoltaic enhancement in the graded structure solar cells, we need to understand the recombination mechanism in the PbS QDHSCs. In the PbS QDHSCs, there are several possible recombination mechanisms. Figure 5a shows the possible recombination processes, including interfacial recombination, trap-assisted recombination, and band-to-band recombination.[31] In this study, we focus on ① interfacial recombination at the PbS/Au contact interface and ② trap-assisted recombination in the PbS QD active layer through an intragap state. After employing the graded structure, the following three effects are anticipated, as shown in Figure 5b: i) The graded structure, as an electron-blocking layer, reduces the interfacial recombination at the PbS/Au interface; ii) The graded structure provides a multi-stage impetus to drive efficiency-limiting electrons towards the TiO_2 electron-transfer layer; and iii) the additional carriers can fill the trap states to reduce the trap-assisted recombination in the PbS QD active layers.

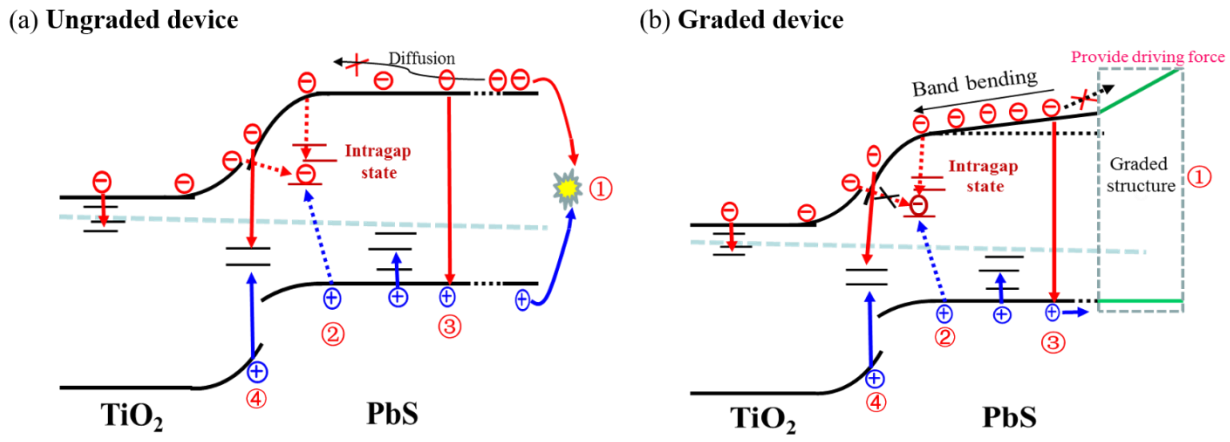

Figure 5. Possible recombination channels for photogenerated carriers in the PbS QDHSCs including ① Interfacial recombination at PbS/gold contact interface, ② Trap-assisted recombination, ③Band to band recombination and ④ Interfacial recombination at TiO_2 /PbS for (a) Ungraded device and (b) Graded devices.

To better understand the improvement in the short-circuit current and the change in the recombination mechanism of the graded structure PbS QDHSCs, we characterized the devices in several ways to investigate their working mechanisms. First, to gain insights into the mechanisms leading to the photovoltaic performance improvements in graded QD devices with different ELA structures, we studied how Jsc and Voc depend on light intensity (P) in these devices (Figure 6a, b). Figure 6a displays the Jsc as a function of the light intensity P_{Light} in a double logarithmic scale. The Jsc values for all devices increased sub-linearly with the light intensity, and the experimental data are fitted with $Jsc(P)=P^{\alpha}_{Light}$,[32]to ascertain the contribution of the charge recombination in the loss mechanism for the photocurrent, where α is the exponential factor (called the recombination coefficient) and is obtained for the ungraded and graded devices from the fitting. If the α value is close to 1, that signifies that nongeminate recombination (such as trap-assisted recombination) at short-circuit conditions is negligible.[32-33] However, if the α value is smaller than 1, both trap-

assisted recombination and interface state recombination are present in the solar cell.[34] In the current case, for the Type I ungraded device and the Type II, III, and IV graded devices, a logarithmic dependence is observed at all ranges of light intensities with α being 0.71, 0.74, 0.78, and 0.75, respectively. The changes in the value of α correspond to the changes in Jsc. In the graded devices, a reduction in the nongeminate recombination is expected because of the decreased trap-assisted recombination in the PbS active layer (process 2 in Figure 5b).

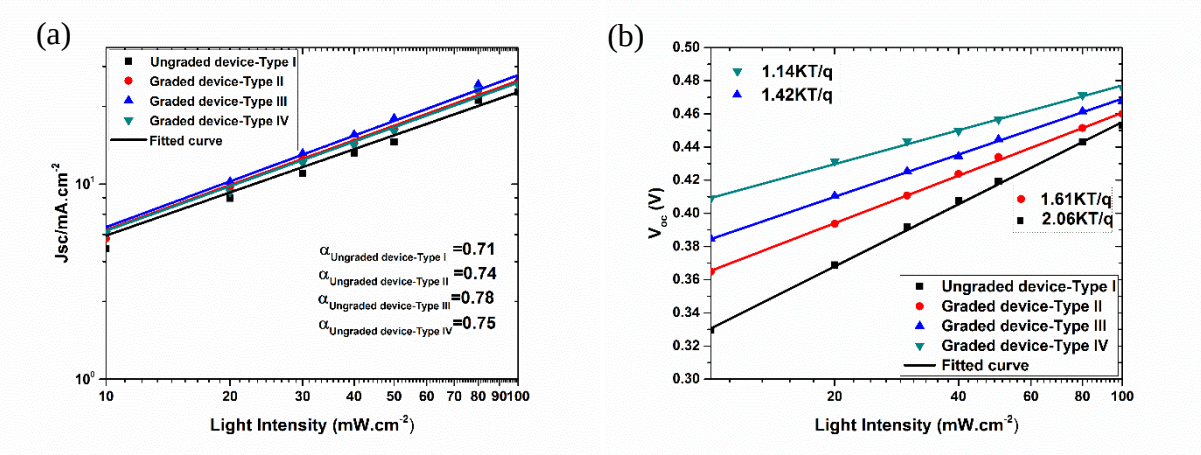

Figure 6. (a) Light-intensity dependence of Jsc and (b) light intensity dependence of Voc for the four types of QDHSCs. The solid lines are the fitting results.

In these solar cells, by investigating the diode ideality factor n, the dominant recombination mechanism could also be determined. Two methods can be used to obtain the ideality factor: one is by fitting the dark J−V curves with the ideal diode equation; the other is by fitting the light intensity dependence of the Voc curves. However, it is hard to ignore the influence of the series resistance in the former method. Using the latter method to determine the ideality factor n is usually considered to be a better estimate since it is not influenced by series resistance and is supposed to reflect the recombination mechanisms under open-circuit conditions.[34] Figure 6b also shows the increase in Voc for the four types of devices with increasing light intensity. For a standard junction

solar cell, neglecting the series and shunt resistances, the light intensity (P_{light}) dependence of the Voc has the following relation:[35-36]

$$V_{oc}(P) = \frac{nkT}{q} ln\left(P_{Light}\right) + C \qquad (2)$$

where k is the Boltzmann constant, T is the temperature, q is the absolute value of electron charge, n is the ideality factor, C is a constant.

By fitting the Voc vs. P_{Light} curves with equation (2), *n* is determined to be 2.06, 1.61, 1.42, and 1.14 for the ungraded device Type I and the graded devices Type II, III, IV, respectively (Figure 6b). The great difference in *n* for different type of the QDHSCs can be interpreted as being due to the different carrier recombination characteristics, reflecting the different J–V characteristics of solar cells with different device structures. Ideally, for a standard p-n junction, when the recombination is dominated by band-to-band recombination where electrons in the conduction band recombine directly with holes in the valence band, the value of the ideality factor *n* is theoretically close to 1. On the other hand, when trap-assisted recombination at the interfaces or through the mid-gap states in the PbS QD active layer dominates, the values n theoretically range from 1 to 2 ($1 < n \leqslant 2$).[36] Our results (Figure 6b) reveal the decrease in the ideality factor from 2.06 (ungraded) to 1.14 (graded) along with the increase in the number of layers of differently size QDs, reflecting that the relative contribution of trap-assisted recombination is reduced. This is because, in the graded structure as shown in Figure 5b, the intrinsic electric field induced by the graded structure increases in the order of Type IV > Type III > Type II. Thus, more charge carriers can be driven with the electric field increasing and more trap states can be filled by charge carriers, which results in the strong suppression of the trap-assisted recombination. Thus, for the graded devices, the ELA structure additionally acts like an increase in incident light intensity. Therefore,

this validates the idea that trap-assisted recombination can be largely suppressed in the graded structure solar cells.

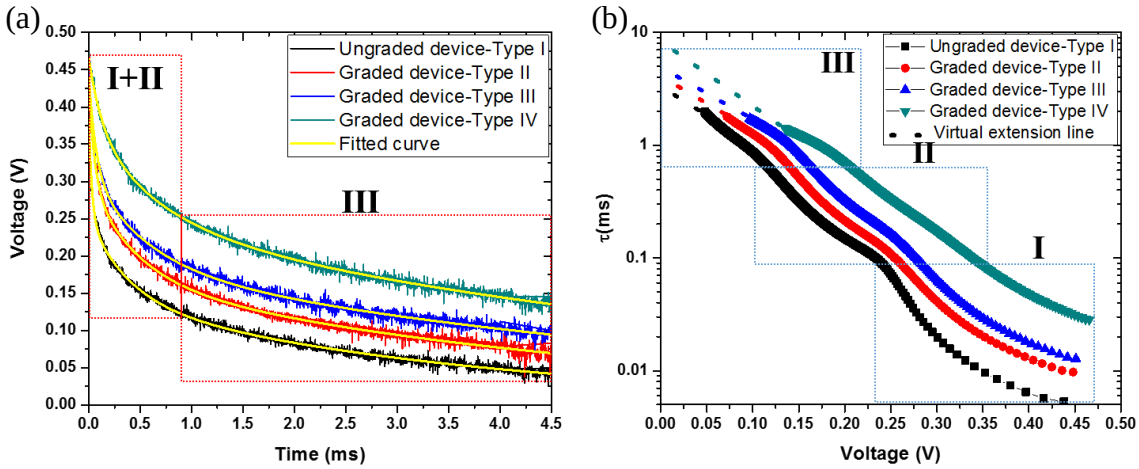

Figure 7. (a) Normalized open-circuit photovoltage decay curves for ungraded and graded PbS QDHSCs, showing three dominant decay processes. (b) The effective carrier lifetimes calculated from the voltage decay curves.

Table 2. Fitted proportionality constants (including the relative weights) and time constants obtained from the open-circuit photovoltage decay curves of the PbS QDHSCs.

Cells	A_1 ($A_1/(A_1+A_2+A_3)$)	τ_1(ms)	A_2 ($A_2/(A_1+A_2+A_3)$)	τ_2(ms)	A_3 ($A_3/(A_1+A_2+A_3)$)	τ_3(ms)
Type I	0.131(34.4%)	0.031±0.001	0.108（28.3%）	0.384±0.001	0.143（37.3%）	3.66±0.01
Type II	0.132(30.5%)	0.056±0.001	0.128（29.8%）	0.457±0.001	0.171（39.7%）	4.98±0.01
Type III	0.126(28.6%)	0.078±0.001	0.124（28.3%）	0.547±0.001	0.190（43.1%）	6.43±0.01
Type IV	0.087(18.8%)	0.127±0.001	0130（27.9%）	0.646±0.001	0.248（53.3%）	7.40±0.01

To directly investigate the possible charge-recombination processes, the transient photovoltage decays were measured. Upon illumination of the PbS QDHSCs by a 532-nm laser pulse at open-

circuit conditions, open-circuit photovoltages of the solar cells are obtained. When the incident laser is switched off, all photogenerated carriers will ultimately recombine, leading to a decay in the photovoltage. The transient photovoltage decay depends on the recombination types and thus gives valuable information on carrier recombination. In addition, to obtain further detail about the effects of intragap states, we measured transient photovoltage decay without background illumination.

Figure 7a shows the transient photovoltage decay behaviours of the ungraded device and the three types of graded devices. The graded cells exhibited much slower decay processes than the ungraded cell, which provided direct proof of reduced recombination and increased carrier lifetime in the graded cells. In addition, for the graded cells, the decay processes slowed with the increase in the top layer number. The decay curves can be roughly divided into three processes, where section I and section II are both fast decay processes and section III is a slow decay process. These photovoltage decay processes correspond to different recombination processes occurring at different timescales. Therefore, the three decay processes suggest that there are at least three recombination mechanisms in this case. We can fit the decay curves very well by using a superposition of three exponential functions as shown in the following equation:

$$y(t) = A_1 e^{-t/\tau_1} + A_2 e^{-t/\tau_2} + A_3 e^{-t/\tau_3} \quad (3)$$

where A_1, A_2 and A_3 are proportionality constants and τ_1, τ_2 and τ_3 are time constants. The fitted curves and the corresponding parameters are shown in Figure 7a (yellow line) and Table 2, respectively. For equation (3), we assigned the first exponential decay to the fastest photovoltage decay process (section I), the second exponential decay to the sub-rapid voltage decay process (section II) and the third exponential decay to the slow photovoltage decay process (section III). Figure S7 shows that in the PbS QDHSCs, when the excitation light is switched off, the

photogenerated free carriers could recombine through three channels: (i) intrinsic trapping-assisted recombination in PbS and the TiO_2 films; (ii) interfacial recombination at the TiO_2/PbS interface defects and PbS/Au interface defects and (iii) direct recombination of photogenerated free electrons in TiO_2 and holes in PbS layers. From our previous research results,[27, 37-38] in the high Voc regime (section I), the value of τ_{eff} was in the ultrafast timescale (~0.1 ms, constant τ_1), and thus, this regime could be related to trap-assisted recombination (process i in Figure S7). In the section II regime, the value of τ_{eff} was more than 0.2 ms (constant τ_2), and this regime could be related to interfacial recombination at the TiO_2/PbS and PbS/gold interfaces (process ii in Figure S7). In the low Voc regime (section III), the value of τ_{eff} was more than 1 ms (constant τ_3); as this regime shows a long time-scale decay process, it could be related to direct recombination of free holes in the PbS layer and free electrons in the TiO_2 layer due to diffusion (process iii in Figure S7).

Table 2 shows the parameters obtained by fitting equation (3) to the Voc decays in Figure 7(a). In section I, the weight of A_1 decreases and the decay time constant τ_1 increases from the Type I device to the Type IV device. This shift reflects the reduction of trap-assisted recombination with the increasing extent of the band bending due to the trap states filling as mentioned above, which is consistent with the ideality n change for different devices. For section II, the weight of A_2 showed no obvious changes, but the decay time constant τ_2 increased continually from Type I to Type IV (process ii in Figure 6b). This could be attributed to the reduction in the recombination at the interfaces of PbS/Au in the ELA structures. The section III decay process represents direct recombination between electrons and holes in the TiO_2 and PbS layers, respectively, where the Voc will disappear completely after this process. As a result of other recombination proportion decreases in the graded cells, the weight of A_3 increased correspondingly. In addition, the decay

time constant τ_3 significantly increased in the graded devices. We suspect that this is probably because more ELA structure layers can cause stronger band bending, which creates a quasi-electric field opposed to the electron diffusion direction in this situation, thus increasing the difficulty of direct recombination of electrons and holes.

The effective carrier lifetime (τ_{eff}) in the PbS QDHSCs from the photovoltage decay can be evaluated as defined by the following equations:[39-40]

$$\tau_{eff} = -\left(\frac{kT}{q}\right)/\frac{dV_{oc}}{dt} = \frac{1}{(\tau_n^{-1}+\tau_p^{-1})} \quad (4)$$

$$\tau_n^{-1} = \frac{(dn/dt)}{n} \quad (5)$$

$$\tau_p^{-1} = \frac{(\mathrm{d}p/dt)}{p} \quad (6)$$

where *k* is the Boltzmann constant, T is the temperature, q is the elementary charge, and n and p are the photoexcited electron and hole carrier densities in the PbS QDHSCs. τ_n and τ_p are the electron and hole lifetimes in the PbS QDHSCs. According to the above equations, the open-circuit photovoltage decay is dependent on both the electron and hole lifetimes in PbS QDHSCs.

As shown in Figure 7b, the photovoltage-dependent effective carrier lifetime could also be divided into three sections, corresponding to the three photovoltage decay processes. Throughout the Voc regime (sections I, II and III in Figure 7b), the values of τ_{eff} in the graded devices were 2–6 times higher than in the ungraded device, in the order of Type IV > Type III > Type II > Type I, which can be understood through the above discussions. Based on these experimental results, the ELA structure was concluded to have three benefits in the Voc decay processes: (i) reducing the interfacial recombination, e.g., at PbS/Au; (ii) reducing the trap-assisted recombination and (iii) slowing the direct recombination of free electrons and holes.

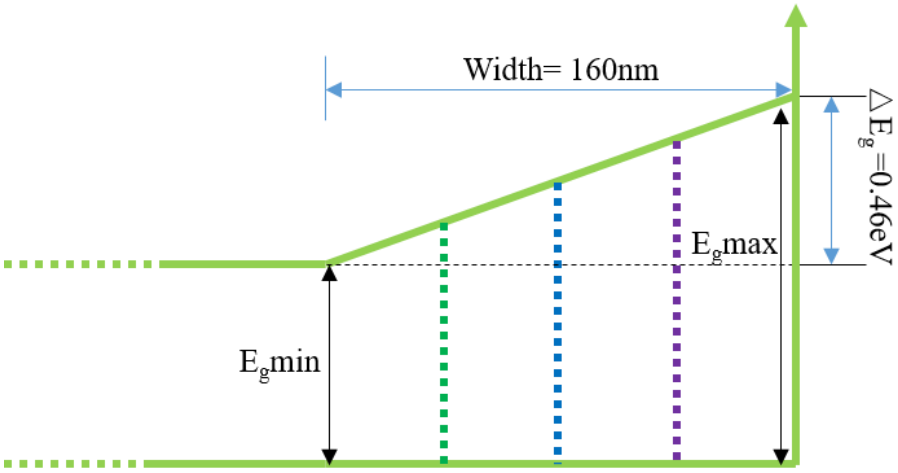

Figure 8. Band diagram for the PbS absorber layer of a graded Type IV device, with linear band-gap variation as a function of position (graded structure thickness).

According to the above analysis, in the graded structure, the carriers have a longer *"diffusion length",* which will increase the probability of charge collection at the heterojunction, thus leading to an increased Jsc. Due to the band bending, the graded structure will provide a force similar to the drift force due to a quasi-electric field. In other words, in the graded device, electrons drift because of the electric field due to the potential variation and by the additional quasi-electric field associated with the conduction band variation with position.[41] Thus, in the case of a graded structure, a drift-diffusion length should be defined. If electron drift and diffusion are in the same direction, the drift-diffusion length will be[42]

$$L_n = \frac{l_n}{\sqrt{1+\left(\frac{\xi_e l_n}{2V_T}\right)^2} - \frac{\xi_e l_n}{2V_T}} \qquad (7)$$

where l_n is the electron diffusion length, V_T is the thermal potential (kT/q) and ξ_e is the quasi-electric field in the ELA region. For the Type IV device (Figure 8), the absorber layer thickness is approximately 300 nm, the diffusion length in the colloidal PbS QD film is (as one report) l_n=80 ± 10 nm,[43] and the total band gap (conduction band) change is ΔEg=0.46 eV. As mentioned above,

the ELA structure can cause the band bending, and here we assume that the ELA structure of the adjacent layer of M-PbS also belong to this quasi-electric field. Thereby the space-charge width for this device could be on the order of 160 nm (1 layer M + 1 layer S1 + 1 layer S2 + 1 layer S3-PbS). Therefore, the quasi-electric field caused by this band gap variation would be approximately ξ_e=2.88×10^4 V/cm directed towards the junction interface. The drift-diffusion length Ln will become approximately 720 nm, which is approximately 9 times the diffusion length (80 nm). Thus, the quasi-electric field attributed to an ELA structure built by differently sized PbS layers in a solar cell should result in a large increase in effective diffusion length.

Furthermore, we have evaluated two important properties, i.e., hysteresis and stability, for our solar cells. Figure S8a shows the hysteresis of our PbS QDHSCs, where no significant hysteretic effect (lower than 1%) is identified. Then, the long-term stability was evaluated without any encapsulation in ambient atmosphere, which was stored under dark conditions without any humidity control, as shown in Figure S8b. Both the ungraded device (Type I) and the graded devices (e.g., Type III) were stable for over 150 days (>3600 h) without any significant degradation, exhibiting excellent long-term storage stability.

3. CONCLUSIONS

In summary, we have demonstrated that the ELA engineering in the active QD layers of QDHSCs can be used to improve the electron collection efficiency at the heterojunction and reduce trap-assisted and interfacial recombination. Through the ELA strategy, a great increase (from 28 mA/cm^2 to 33 mA/cm^2) in Jsc and a maximum efficiency of 7.24% (the active area is 16 mm^2) have been achieved by optimization of the structure. Grading the energy level does not cause much variation in the optical absorption, but it can improve the collection of photogenerated carriers. The ELA produces spatial decoupling of the electron and hole profiles, resulting in an effective

increase in the photoexcited carrier lifetime. This is directly linked to the enhanced effective diffusion length and increased Jsc. In our study, recombination mechanisms in PbS QDHSCs were investigated by examining the light intensity dependence of Jsc and Voc and the transient voltage decay. Our results show that the ELA structure has two benefits for QDHSCs: (i) The ELA structure, as an electron-blocking layer, reduces the interfacial recombination at the PbS/Au interface; (ii) The ELA structure can drive more electron carriers towards the electron transfer layer, and the additional electron carriers can fill the trap states, reducing the trap-assisted recombination in the PbS QDHSCs. With the increase in the number of graded structure layers, the electron driving force becomes stronger, leading to longer minority carrier lifetimes. However, the graded Type IV device has the longest carrier lifetime but does not have the best performance. This is because the presence of the graded structure causes gradual resistance increase by introducing undesirable band bending between the valence band of the M-size PbS layer and the gold contact. In the Type IV device, this barrier is hard to ignore, which seriously affected the transport of holes to the gold contact. Through the band energy engineering strategy and the optimization of the thickness of the graded structure, the Type III device achieved the best efficiency. The device stability and hysteresis were also evaluated. Negligible hysteretic effects were observed in our devices, and they exhibited excellent storage stability in air (without any performance decline over 150 days). In short, this study highlights the significance of band energy engineering in achieving high-efficiency planar heterojunction QD solar cells. The charge recombination mechanisms characterized in this work may be able to shed light on further improvements of QDHSCs and/or other types of solar cells. This study suggests a useful strategy to improve the effective diffusion lengths and photogenerated carriers of PbS QDHSCs via simple architecture design.

4. EXPERIMENTAL SECTION

4.1. Materials. Lead (II) oxide (Wako, 99.5%), oleic acid (OA, Wako, 60%), 1-octadecene (ODE, Aldrich, 90%), and bis (trimethylsilyl) sulfide (TMS2 sulfide, Aldrich, 99.999%), Cadmium chloride (CdCl2, Wako, 99.8%), Oleylamine (OLA, Aldrich, 70%), Tetradecylphosphonic acid (TDPA, Aldrich, 97%), Titanium diisopropoxide bis(acetylacetonate) (75 wt %, Aldrich), 1-butanol (Wako, 99%) were used as purchased without further purification.

4.2. PbS quantum dot synthesis. Colloidal PbS QDs were synthesized according to a modified literature method,[23] various sizes of PbS QDs were prepared as described previously in literature.[44] In this work, PbS QDs were manipulated using the standard Schlenk line techniques.[6] The mixed solution of 6 mmol PbO and 15 mmol OA and 50 ml of ODE in a 100 mL three-neck flask was stirred and degassed at room temperature and 80 °C for 20 min and 40 min, successively. The solution was then heated for 1 h up to 120 °C under a nitrogen atmosphere, then the solution was allowed to cool down to the required temperatures of 115, 105, 75, and 69 °C, followed by the injection of TMS solution (3 mmol TMS mixed with 10 mL pre-degassed ODE). After injection, the heater was removed immediately while the solution was kept stirring. When the solution was cooled down to 75 °C, a $CdCl_2$-TDPA-OLA solution containing 1 mmol $CdCl_2$, 0.1 mmol TDPA, and 3 mL OLA was injected into the PbS colloid. After cooling down to room temperature, PbS QDs were precipitated from the growth mixture and re-dispersed into an organic solvent toluene. The resulting precipitate was isolated by centrifugation, washed twice with acetone to remove the unbound OA ligands in PbS colloid, and then was dispersed in octane. The concentration of PbS colloid was approximately 100 $mg \cdot ml^{-1}$ assuming that the reactant TMS was completely transformed into the PbS product.

4.3. TiO_2 compact layer synthesis. Thin TiO_2 compact layer was coated on FTO glass (25 mm × 25 mm). The TiO_2 compact film was prepared according to a standard procedure which has been reported in the literature.[45] To prepare the precursor solution, 1.46 mL of Titanium diisopropoxide bis(acetylacetonate) and 10 mL of 1-butanol were stirred at room temperature for 30min. To form a sol, the solution should be filtered by 0.1 μm filter. A compact TiO_2 film was coated by spin-coating method with a low speed of 1000 rpm for 2s and at a high speed of 3000 rpm for 30s. The thickness of the TiO_2 compact film was controlled by the high speed of the spin coater. After spin coating, the film was thermally annealed at 500 °C for 30 min.

4.4. Device fabrication. To fabricate PbS heterojunction solar cells, PbS colloidal QDs were prepared on TiO_2 electrodes by a typical layer-by-layer method using a fully automatic spin-coater under ambient conditions. Each PbS colloidal layer was deposited at 2500 rpm and ligand exchange briefly with CTAB solution (30mM in methanol) was conducted by spin-cast at 2500 rpm. The ligand exchange step was conducted twice to ensure complete ligand exchange with the oleic acid capped on PbS surfaces. Each layer was then rinsed three times with methanol while spinning at 2500 rpm to remove excess unbound ligands. Then the QD spin procedure was repeated until desired thickness was reached. Contacts consisting of ~100 nm of gold were deposited on the PbS layer through a mask to create four identical cells on each substrate by thermal evaporation. The contact sizes were 0.16 cm^2.

4.5. Characterization

The current density-voltage (J-V) measurements were performed using a Keithley 2400 source meter under dark and AM 1.5 with solar simulator PEC-L10. The IPCE spectra were measured under illumination using a Nikon G250 monochromator equipped with a 300 W Xenon arc lamp. The transient open-circuit voltage decay measurements were carried out using a 630-nm diode

laser with the pulse duration of 5 ns and repetition rate of 4 Hz. The voltage responses were recorded using an Iwatsu digital oscilloscope DS-5554. The transient voltage decay measurements were taken without a background light bias.

ASSOCIATED CONTENT

Supporting Information

J-V characteristics with four PbS layer thicknesses; histogram of the Jsc of the type I and type III devices; Band diagram of the type IV device; Dark J-V curves; Absorptions spectra of the PbS absorber layers; Spatial band diagrams and J-V characteristics; table summarizing the statistical average of the photovoltaic performance parameters; carrier transport and recombination of the Voc decay process; J–V curves measured by forward and reverse scans and stability evaluation diagram(PDF)

Corresponding Author

*Tel: 81-0424435464; e-mail: shen@pc.uec.ac.jp (Qing Shen).

Author Contributions

The manuscript was written through contributions of all authors. All authors have given approval to the final version of the manuscript.

Notes

The authors declare no competing financial interest.

ACKNOWLEDGMENT

This research was supported by the Japan Science and Technology Agency (JST) CREST and PRESTO program and MEXT KAKENHI grant numbers 26286013 and 17H02736, and by the China Scholarship Council (CSC) of china grant number 201608050109.

REFERENCES

1. Peng, Z. A.; Peng, X., Formation of High-Quality CdTe, CdSe, and CdS Nanocrystals Using CdO as Precursor. *J. Am. Chem. Soc.* **2001,** *123*, 183-184.
2. Pattantyus-Abraham, A. G.; Kramer, I. J.; Barkhouse, A. R.; Wang, X. H.; Konstantatos, G.; Debnath, R.; Levina, L.; Raabe, I.; Nazeeruddin, M. K.; Gratzel, M.; Sargent, E. H., Depleted-Heterojunction Colloidal Quantum Dot Solar Cells. *Acs Nano* **2010,** *4*, 3374-3380.
3. McGuire, J. A.; Joo, J.; Pietryga, J. M.; Schaller, R. D.; Klimov, V. I., New Aspects of Carrier Multiplication in Semiconductor Nanocrystals. *Acc. Chem. Res.* **2008,** *41*, 1810-1819.
4. Wise, F. W., Lead Salt Quantum Dots: the Limit of Strong Quantum Confinement. *Acc. Chem. Res.* **2000,** *33*, 773-780.
5. Zaban, A.; Mićić, O. I.; Gregg, B. A.; Nozik, A. J., Photosensitization of Nanoporous TiO_2 Electrodes with InP Quantum Dots. *Langmuir* **1998,** *14*, 3153-3156.
6. Chuang, C.-H. M.; Brown, P. R.; Bulović, V.; Bawendi, M. G., Improved Performance and Stability in Quantum Dot Solar Cells through Band Alignment Engineering. *Nat. Mater.* **2014,** *13*, 796-801.
7. Lan, X.; Voznyy, O.; Kiani, A.; García de Arquer, F. P.; Abbas, A. S.; Kim, G.-H.; Liu, M.; Yang, Z.; Walters, G.; Xu, J.; Yuan, M.; Ning, Z.; Fan, F.; Kanjanaboos, P.; Kramer, I.; Zhitomirsky, D.; Lee, P.; Perelgut, A.; Hoogland, S.; Sargent, E. H., Passivation Using Molecular Halides Increases Quantum Dot Solar Cell Performance. *Adv. Mater.* **2016,** *28*, 299-304.
8. Kim, G.-H.; García de Arquer, F. P.; Yoon, Y. J.; Lan, X.; Liu, M.; Voznyy, O.; Yang, Z.; Fan, F.; Ip, A. H.; Kanjanaboos, P.; Hoogland, S.; Kim, J. Y.; Sargent, E. H., High-Efficiency Colloidal Quantum Dot Photovoltaics via Robust Self-Assembled Monolayers. *Nano Lett.* **2015,** *15*, 7691-7696.
9. Lan, X.; Voznyy, O.; García de Arquer, F. P.; Liu, M.; Xu, J.; Proppe, A. H.; Walters, G.; Fan, F.; Tan, H.; Liu, M.; Yang, Z.; Hoogland, S.; Sargent, E. H., 10.6% Certified Colloidal Quantum Dot Solar Cells via Solvent-Polarity-Engineered Halide Passivation. *Nano Lett.* **2016,** *16*, 4630-4634.
10. Kim, Y.; Bicanic, K.; Tan, H.; Ouellette, O.; Sutherland, B. R.; García de Arquer, F. P.; Jo, J. W.; Liu, M.; Sun, B.; Liu, M.; Hoogland, S.; Sargent, E. H., Nanoimprint-Transfer-Patterned Solids Enhance Light Absorption in Colloidal Quantum Dot Solar Cells. *Nano Lett.* **2017**, 17, pp 2349–2353.
11. Adinolfi, V.; Ning, Z.; Xu, J.; Masala, S.; Zhitomirsky, D.; Thon, S. M.; Sargent, E. H., Electric Field Engineering Using Quantum-Size-Effect-Tuned Heterojunctions. *Appl. Phys. Lett.* **2013,** *103*, 011106.

12. Ning, Z.; Ren, Y.; Hoogland, S.; Voznyy, O.; Levina, L.; Stadler, P.; Lan, X.; Zhitomirsky, D.; Sargent, E. H., All-Inorganic Colloidal Quantum Dot Photovoltaics Employing Solution-Phase Halide Passivation. *Adv. Mater.* **2012,** *24*, 6295-6299.
13. Kramer, I. J.; Levina, L.; Debnath, R.; Zhitomirsky, D.; Sargent, E. H., Solar Cells Using Quantum Funnels. *Nano Lett.* **2011,** *11*, 3701-3706.
14. Jang, J.; Song, J. H.; Choi, H.; Baik, S. J.; Jeong, S., Photovoltaic Light Absorber with Spatial Energy Band Gradient Using PbS Quantum Dot Layers. *Sol. Energy Mater. Sol. Cells* **2015,** *141*, 270-274.
15. Zhang, X.; Zhang, Y.; Yan, L.; Wu, H.; Gao, W.; Zhao, J.; Yu, W. W., PbSe Nanocrystal Solar Cells Using Bandgap Engineering. *RSC Adv.* **2015,** *5*, 65569-65574.
16. Kim, J. Y.; Adinolfi, V.; Sutherland, B. R.; Voznyy, O.; Kwon, S. J.; Kim, T. W.; Kim, J.; Ihee, H.; Kemp, K.; Adachi, M.; Yuan, M.; Kramer, I.; Zhitomirsky, D.; Hoogland, S.; Sargent, E. H., Single-step Fabrication of Quantum Funnels via Centrifugal Colloidal Casting of Nanoparticle Films. *Nat. Commun.* **2015,** *6*, 7772.
17. Ning, Z.; Zhitomirsky, D.; Adinolfi, V.; Sutherland, B.; Xu, J.; Voznyy, O.; Maraghechi, P.; Lan, X.; Hoogland, S.; Ren, Y.; Sargent, E. H., Graded Doping for Enhanced Colloidal Quantum Dot Photovoltaics. *Adv. Mater.* **2013,** *25*, 1719-1723.
18. Santra, P. K.; Palmstrom, A. F.; Tanskanen, J. T.; Yang, N.; Bent, S. F., Improving Performance in Colloidal Quantum Dot Solar Cells by Tuning Band Alignment through Surface Dipole Moments. *J. Phys. Chem. C* **2015,** *119*, 2996-3005.
19. Malik, R. J.; Capasso, F.; Stall, R. A.; Kiehl, R. A.; Ryan, R. W.; Wunder, R.; Bethea, C. G., High‐Gain, High‐Frequency AlGaAs/GaAs Graded Band-Gap Base Bipolar Transistors with a Be Diffusion Setback Layer in the Base. *Appl. Phys. Lett.* **1985,** *46*, 600-602.
20. Konagai, M.; Takahashi, K., Graded‐Band‐Gap $pGa_{1-x}Al_xAs$-nGaAs Heterojunction Solar Cells. *J. Appl. Phys.* **1975,** *46*, 3542-3546.
21. Dullweber, T.; anna, G. H.; Rau, U.; Schock, H. W., A New Approach to High-Efficiency Solar Cells by Band Gap Grading in $Cu(In,Ga)Se_2$ Chalcopyrite Semiconductors. *Sol. Energy Mater. Sol. Cells* **2001,** *67*, 145-150.
22. Nelson, J. Over the Limit: Strategies for High Efficiency. *The Physics of Solar Cells*, Imperial College Press: London, **2003,** pp 289-325.
23. Tang, J.; Kemp, K. W.; Hoogland, S.; Jeong, K. S.; Liu, H.; Levina, L.; Furukawa, M.; Wang, X.; Debnath, R.; Cha, D.; Chou, K. W.; Fischer, A.; Amassian, A.; Asbury, J. B.; Sargent, E. H., Colloidal-Quantum-Dot Photovoltaics using Atomic-Ligand Passivation. *Nat. Mater.* **2011,** *10*, 765-771.
24. Moreels, I.; Lambert, K.; Smeets, D.; De Muynck, D.; Nollet, T.; Martins, J. C.; Vanhaecke, F.; Vantomme, A.; Delerue, C.; Allan, G.; Hens, Z., Size-Dependent Optical Properties of Colloidal PbS Quantum Dots. *ACS Nano* **2009,** *3*, 3023-3030.
25. Miller, E. M.; Kroupa, D. M.; Zhang, J.; Schulz, P.; Marshall, A. R.; Kahn, A.; Lany, S.; Luther, J. M.; Beard, M. C.; Perkins, C. L.; van de Lagemaat, J., Revisiting the Valence and Conduction Band Size Dependence of PbS Quantum Dot Thin Films. *ACS Nano* **2016,** *10*, 3302-3311.
26. Shockley, W.; Queisser, H. J., Detailed Balance Limit of Efficiency of p-n Junction Solar Cells. *J. Appl. Phys.* **1961,** *32*, 510-519.
27. Chang, J.; Kuga, Y.; Mora-Sero, I.; Toyoda, T.; Ogomi, Y.; Hayase, S.; Bisquert, J.; Shen, Q., High Reduction of Interfacial Charge Recombination in Colloidal Quantum Dot Solar Cells by Metal Oxide Surface Passivation. *Nanoscale* **2015,** *7*, 5446-5456.

28. Sun, B.; Voznyy, O.; Tan, H.; Stadler, P.; Liu, M.; Walters, G.; Proppe, A. H.; Liu, M.; Fan, J.; Zhuang, T.; Li, J.; Wei, M.; Xu, J.; Kim, Y.; Hoogland, S.; Sargent, E. H., Pseudohalide-Exchanged Quantum Dot Solids Achieve Record Quantum Efficiency in Infrared Photovoltaics. *Adv. Mater.***2017**,29,1700749.
29. Servaites, J. D.; Yeganeh, S.; Marks, T. J.; Ratner, M. A., Efficiency Enhancement in Organic Photovoltaic Cells: Consequences of Optimizing Series Resistance. *Adv. Funct. Mater.* **2010,** *20*, 97-104.
30. Kawawaki, T.; Wang, H.; Kubo, T.; Saito, K.; Nakazaki, J.; Segawa, H.; Tatsuma, T., Efficiency Enhancement of PbS Quantum Dot/ZnO Nanowire Bulk-Heterojunction Solar Cells by Plasmonic Silver Nanocubes. *ACS Nano* **2015,** *9*, 4165-4172.
31. Ehrler, B.; Musselman, K. P.; Böhm, M. L.; Morgenstern, F. S. F.; Vaynzof, Y.; Walker, B. J.; MacManus-Driscoll, J. L.; Greenham, N. C., Preventing Interfacial Recombination in Colloidal Quantum Dot Solar Cells by Doping the Metal Oxide. *ACS Nano* **2013,** *7*, 4210-4220.
32. Gao, F.; Li, Z.; Wang, J.; Rao, A.; Howard, I. A.; Abrusci, A.; Massip, S.; McNeill, C. R.; Greenham, N. C., Trap-Induced Losses in Hybrid Photovoltaics. *ACS Nano* **2014,** *8*, 3213-3221.
33. Riedel, I.; Parisi, J.; Dyakonov, V.; Lutsen, L.; Vanderzande, D.; Hummelen, J. C., Effect of Temperature and Illumination on the Electrical Characteristics of Polymer–Fullerene Bulk-Heterojunction Solar Cells. *Adv. Funct. Mater.* **2004,** *14*, 38-44.
34. Sun, Z.; Sitbon, G.; Pons, T.; Bakulin, A. A.; Chen, Z., Reduced Carrier Recombination in PbS - $CuInS_2$ Quantum Dot Solar Cells. *Sci. Rep.* **2015,** *5*, 10626.
35. Cowan, S. R.; Roy, A.; Heeger, A. J., Recombination in Polymer-Fullerene Bulk Heterojunction Solar Cells. *Phys. Rev.B* **2010,** *82*, 245207.
36. Kemp, K. W.; Labelle, A. J.; Thon, S. M.; Ip, A. H.; Kramer, I. J.; Hoogland, S.; Sargent, E. H., Interface Recombination in Depleted Heterojunction Photovoltaics based on Colloidal Quantum Dots. *Adv. Energy Mater.* **2013,** *3*, 917-922.
37. Zhang, Y.; Ding, C.; Wu, G.; Nakazawa, N.; Chang, J.; Ogomi, Y.; Toyoda, T.; Hayase, S.; Katayama, K.; Shen, Q., Air Stable PbSe Colloidal Quantum Dot Heterojunction Solar Cells: Ligand-Dependent Exciton Dissociation, Recombination, Photovoltaic Property, and Stability. *J. Phys. Chem. C* **2016,** *120*, 28509-28518.
38. Zhang, Y.; Wu, G.; Mora-Seró, I.; Ding, C.; Liu, F.; Huang, Q.; Ogomi, Y.; Hayase, S.; Toyoda, T.; Wang, R.; Otsuki, J.; Shen, Q., Improvement of Photovoltaic Performance of Colloidal Quantum Dot Solar Cells Using Organic Small Molecule as Hole-Selective Layer. *J. Phys. Chem. Lett.* **2017,** 2163-2169.
39. Berry, W. B.; Longrigg, P., Open-Circuit Voltage Decay — Measures of Amorphous Silicon Material Stability and Module Degradation. *Sol. Cells* **1988,** *24*, 321-328.
40. Zaban, A.; Greenshtein, M.; Bisquert, J., Determination of the Electron Lifetime in Nanocrystalline Dye Solar Cells by Open-Circuit Voltage Decay Measurements. *Chemphyschem* **2003,** *4*, 859-864.
41. Benmir, A.; Aida, M. S., Analytical Modeling and Simulation of CIGS Solar Cells. *Energy Procedia* **2013,** *36*, 618-627.
42. Morales-Acevedo, A., Variable Band-Gap Semiconductors as the Basis of New Solar Cells. *Sol. Energy* **2009,** *83*, 1466-1471.
43. Zhitomirsky, D.; Voznyy, O.; Hoogland, S.; Sargent, E. H., Measuring Charge Carrier Diffusion in Coupled Colloidal Quantum Dot Solids. *ACS Nano* **2013,** *7*, 5282-5290.

44. Choi, H.; Ko, J.-H.; Kim, Y.-H.; Jeong, S., Steric-Hindrance-Driven Shape Transition in PbS Quantum Dots: Understanding Size-Dependent Stability. *J. Am. Chem. Soc.* **2013,** *135*, 5278-5281.
45. Jena, A. K.; Chen, H.-W.; Kogo, A.; Sanehira, Y.; Ikegami, M.; Miyasaka, T., The Interface between FTO and the TiO_2 Compact Layer Can Be One of the Origins to Hysteresis in Planar Heterojunction Perovskite Solar Cells. *ACS Appl. Mater. Inter.* **2015,** *7*, 9817-9823.

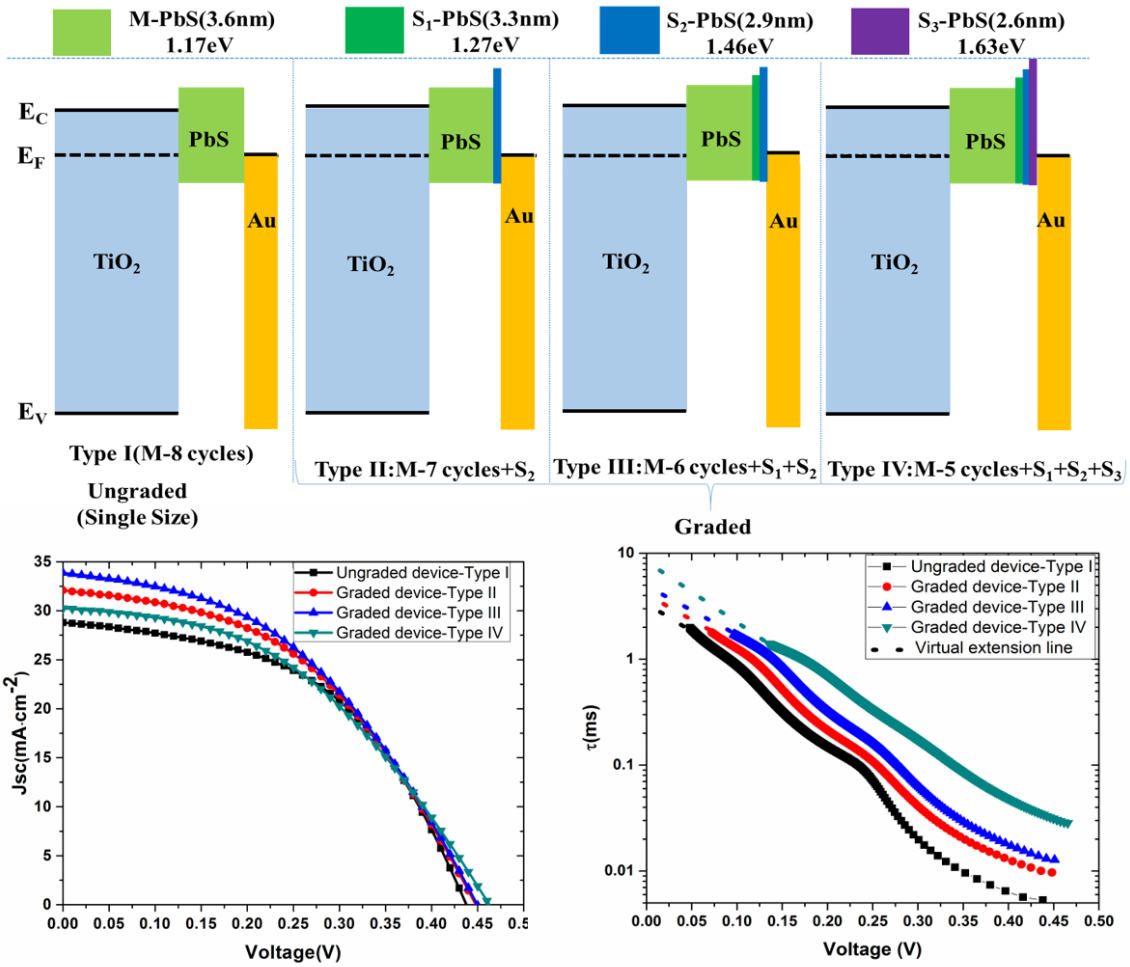
M-PbS(3.6nm)
1.17eV
S1-PbS(3.3nm)
1.27eV
S2-PbS(2.9nm)
1.46eV
S3-PbS(2.6nm)
1.63eV
EC
EF
EV
PbS
Au
TiO2
Type I(M-8 cycles)
Type II:M-7 cycles+S2
Type III:M-6 cycles+S1+S2
Type IV:M-5 cycles+S1+S2+S3
Ungraded
(Single Size)
Graded
Ungraded device-Type I
Graded device-Type II
Graded device-Type III
Graded device-Type IV
Virtual extension line
Jsc(mA·cm-2)
Voltage(V)
τ(ms)
Voltage (V)

TOC